Photon Energy Recovery for Crosstalk Correction in Simultaneous ^{99m}Tc/^{201}Tl Imaging

Pascal Hannequin, Jacky Mas, and Guido Germano

Centre d'Imagerie Nucléaire, Annecy; Service de Médecine Nucléaire, Épinal, France; and Department of Medical Physics and Imaging, Cedars-Sinai Medical Center, Los Angeles, California

Simultaneous ^{99m}Tc sestamibi/^{201}Tl imaging enables the acquisition of images of myocardial stress perfusion and myocardial viability in a single process. One of the major limits of this technique is the crosstalk of the ^{99m}Tc downscattered photons into the ^{201}Tl window. We propose using the spectral deconvolution technique photon energy recovery (PER) for correcting this crosstalk. **Methods:** A planar line phantom made of ^{99}Tc vertical lines and ^{201}Tl horizontal lines and a cardiac SPECT phantom including an anterior (2 mL) and an inferior (1.5 mL) myocardial fixed defect were used. The phantoms were filled with an initial ^{99m}Tc/^{201}Tl ratio of 5:1. Several successive acquisitions were made from time t = 0 to time t = 48 h (^{99m}Tc/^{201}Tl ratio ≈ 0) without moving the phantoms. Total number of counts, contrast, and normalized SD (NSD) were calculated on the Tl-raw and the Tl-PER planar images. SPECT datasets were analyzed. The Tl-raw images recorded at 48 h were considered the reference "virgin" ^{201}Tl images. **Results:** Total number of counts, contrast, and NSD ranged from 336% to 201%, 15% to 29%, and 257% to 225% of the virgin ^{201}Tl values, respectively, for Tl-raw planar images; whereas values for Tl-PER images ranged from 128% to 108%, 61% to 79%, and 154% to 108%, respectively. Anterior and inferior defect contrasts ranged from 1.18 to 1.22 and 1.12 to 1.16 for Tl-raw SPECT images, respectively; whereas for Tl-PER images, value ranges were 1.28–1.32 and 1.21–1.24, respectively. The corresponding reference virgin ^{201}Tl values were 1.31 and 1.25 respectively. Summed score, average defect severity, and average defect extent ranges were 4–5, 0.4–0.52, and 4.7–5.9 for Tl-raw images, respectively, and 8–9, 0.59–0.79, and 7.4–8.8 for Tl-PER images. The reference virgin ^{201}Tl values were 9, 0.73, and 8.7, respectively. **Conclusion:** PER is quantitatively efficient to remove ^{99m}Tc crosstalk photons from ^{201}Tl images for ^{99m}Tc/^{201}Tl ratios ranging from 5:1 to 2:1.

Key Words: simultaneous dual-isotope imaging; crosstalk correction; ^{99m}Tc-sestamibi; ^{201}Tl; SPECT

J Nucl Med 2000; 41:728–736

Simultaneous dual-isotope scintigraphy (SDIS) consists of recording images from 2 different radionuclides at the same time using 1 acquisition. The potential benefits of SDIS are well known. It allows simultaneous evaluation of the processes targeted by the 2 radionuclides, decreases the study time and the probability of patient motion, and yields perfectly registered image pairs. SDIS using various radionuclide pairs has been proposed with both emission–emission and emission–transmission studies (*1,2*).

^{99m}Tc/^{201}Tl SDIS is of great clinical interest because of the well-established usefulness of the separate rest ^{201}Tl–stress ^{99m}Tc-sestamibi protocol in routine myocardial imaging (*3*). In nuclear cardiology, this combination of isotopes has also been proposed for simultaneous ^{99m}Tc blood-pool–^{201}Tl myocardial perfusion imaging (*4*) and for simultaneous ^{99m}Tc infarction–^{201}Tl myocardial perfusion imaging (*5*). It is also of clinical interest in nuclear oncology for parathyroid adenoma (*6*), hepatocellular carcinoma (*7*), and brain tumor imaging (*8*). Moreover, simultaneous ^{99m}Tc/^{201}Tl imaging is used in several emission–transmission protocols in which attenuation of ^{201}Tl photons is corrected using a ^{99m}Tc transmission source (*9,10*). The main limitation of simultaneous ^{99m}Tc/^{201}Tl imaging is the crosstalk of photons from one radionuclide into the acquisition window of the other (*11*).

The effects of crosstalk in simultaneous ^{99m}Tc/^{201}Tl imaging have been investigated by several groups (*12–17*). In myocardial SPECT, crosstalk from primary and scattered high-energy (167 keV) ^{201}Tl photons into the ^{99m}Tc acquisition window (centered on 140 keV) is very small (*14,15*) and is not corrected in practice when performing sequential (separate) rest ^{201}Tl–stress ^{99m}Tc-sestamibi SPECT acquisition. On the contrary, the effect of ^{99m}Tc scattered photons into the ^{201}Tl acquisition window (centered on 70 keV) is substantial (*14–17*), except in the case of large cardiac defects (*12*) or very low ^{99m}Tc/^{201}Tl ratios (*13*). This necessitates the use of correction techniques for removing the ^{99m}Tc scattered photons from the ^{201}Tl window.

Most of the proposed correction procedures (*18–20*) are based on the estimation of ^{99m}Tc crosstalk and its subsequent subtraction from the ^{201}Tl image. This estimation can be performed using a fraction (crosstalk fraction) of the ^{99m}Tc 140-keV image (*6,9,10*) or a fraction of a third image acquired in a spectral window located between the 70- and the 140-keV spectral windows (typically at 100 keV) (*20*). One limitation of this approach is the difficulty in calculating the crosstalk fraction, as well as the assumption that the spatial distribution of the ^{99m}Tc scattered photons in the image acquired at 100 or 140 keV is the same as that in the 70-keV image. Another technique, based on a spatial

Received May 7, 1999; revision accepted Aug. 24, 1999.

For correspondence or reprints contact: Pascal Hannequin, MD, PhD, Centre d'Imagerie Nucléaire, 4 Chemin de la Tour de la Reine, 74000 Annecy, France.

deconvolution using the ^{99m}Tc point spread function, has been proposed (*2,21*). However, this technique theoretically requires recording the point-spread functions at different water depths and adding regularization procedures. To date, no crosstalk correction procedure has been validated in clinical practice.

We have developed a spectral deconvolution technique, called photon energy recovery (PER) that improves the effective energy resolution of γ cameras (*22*). PER allows the selection of photons according to their true energy and then separates the unscattered from the scattered ones. The technique has already been validated for scatter removal in single-isotope ^{99m}Tc studies (*23*). Because crosstalk is a form of scatter, we hypothesized that PER could be applied to ^{99m}Tc crosstalk correction in simultaneous ^{99m}Tc/^{201}Tl acquisition. This work is a validation study of that hypothesis, using a planar line phantom and a cardiac SPECT phantom.

MATERIALS AND METHODS

PER for Scatter Removal in Single-Isotope Imaging with ^{99m}Tc

Theory. The principle of PER for a single monopeak radionuclide study (*22*) is that the detected spectrum (DS) at each pixel is a linear combination of the spectrum of the primary photons (PS) and that of the scattered photons (SS) can be expressed as:

$$DS = p\,PS + s\,SS, \qquad \text{Eq. 1}$$

where p and s are the number of primary and scattered photons, respectively. These 2 coefficients can easily be estimated using classical linear regression, provided that spectra PS and SS are known.

In PER, these spectra are computed using the energy impulse response (EIR) of the detector. The EIR of the detector for the photons of energy e (EIR_e) is postulated to be a Gaussian function with a mean = e and an SD = (er)/c, where r is the energy resolution of the detector and c is the constant $2[2\log(2)]^{1/2}$. The energy resolution r at energy e is the ratio of full width at half maximum to e (FWHM/e). PS is assumed to be the EIR at photopeak energy, and SS is assumed to be the weighted sum of all EIRs at energies lower than the photopeak energy. Only the EIRs that contribute significantly to the spectral acquisition window are included in the summation. For example, using the conventional 126- to 154-keV ^{99m}Tc window:

$$PS = EIR_{140}, \qquad \text{Eq. 2}$$

and

$$SS = \sum_{e=115}^{139} w_e\,EIR_e, \qquad \text{Eq. 3}$$

where w_e is the weight of EIR_e in this summation.

The coefficients w_e are estimated using the following iterative process. A first estimation of the coefficients p and s is calculated assuming that the distribution of the weighting coefficients w_e is uniform, i.e., that all the EIRs in Equation 3 have weight = 1. This hypothesis is only an initial approximation for the shape of the SS. This first estimation for p and s is then refined using an iterative process that consists of adjusting the shape of the SS (i.e., recalculating the coefficients w_e) to minimize the distance (DIST) between the DS and the reconstructed spectrum (RS). At step m:

$$^{m}RS = {}^{m}p\,EIR_{140} + {}^{m}s\,{}^{m}SS, \qquad \text{Eq. 4}$$

where ^{m}RS is the RS at step m, ^{m}SS is the adjustment of SS at step m, and ^{m}p and ^{m}s are the estimations at step m of p and s, respectively.

Considering the characteristics of the noise in the scintigraphic data (the SD of the distribution = the square root of the mean), the differences between the DS values and the RS values have been expressed as numbers of SDs of the DS values. In this way, the distance between the DS and the ^{m}RS at step m is defined as the mean number of SDs, using the following expression:

$$^{m}DIST = \frac{1}{N}\sum_{E=1}^{N}\frac{ABS[DS(E) - {}^{m}RS(E)]}{[DS(E)]^{1/2}}, \qquad \text{Eq. 5}$$

where N is the number of energy intervals of the DS and RS. DS(E) and ^{m}RS(E) are the values of the DS and RS at energy E, respectively.

Adopting the usual 5% level of significance for statistical tests and the standardized normal distribution table, it has been chosen to stop the iterative process when $^{m}DIST < 1.96$ (2, in practice) SDs. However, Monte Carlo simulations have shown that PER is stable and converges well with a small number (10–15) of iterations (*22*). The calculation of p and s is performed for all the pixels in the image.

Figure 1A shows an example of ^{99m}Tc DS and RS in 2 pixels extracted from the first projection of a ^{99m}Tc cardiac phantom SPECT study with 3 energy subwindows. One pixel is a high-count-level pixel located over the myocardium, and 1 is a low-count-level pixel located over the tissue background. This figure illustrates the good fit with the PER model, both at low and high statistical noise levels.

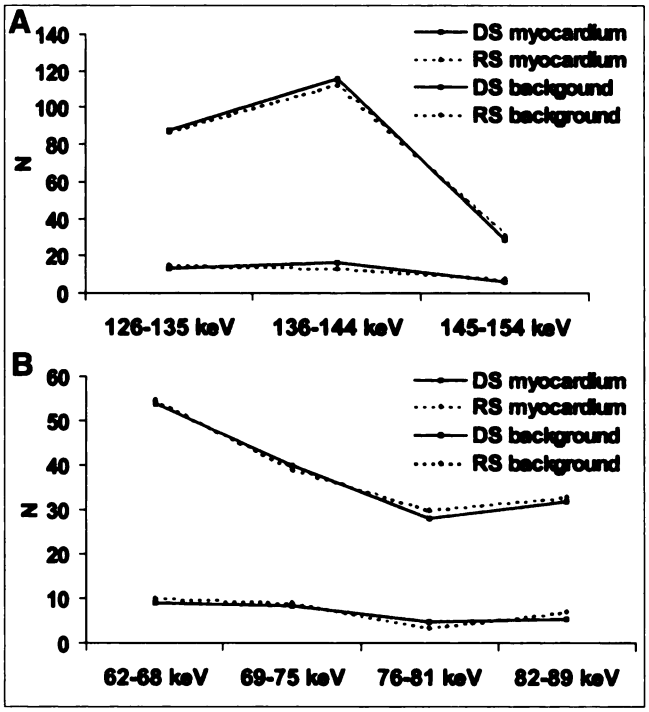

FIGURE 1. (A) ^{99m}Tc DS and RS in myocardium pixel (high count level) and tissue-background pixel (low count level) extracted from ^{99m}Tc cardiac phantom SPECT study. (B) ^{201}Tl DS and RS in same pixels extracted from simultaneous ^{99m}Tc/^{201}Tl cardiac phantom SPECT study (^{99m}Tc/^{201}Tl ratio = 2).

Implementation. The N of energy intervals (which is the number of equations in the system) must be at least equal to the number of unknowns in the system. However, N must not be too high to keep an adequate count level in each energy subwindow. The number of unknowns in Equation 1 is 2, and 3 energy subwindows (N = 3) are used. In practice, the conventional 126- to 154-keV ^{99m}Tc photopeak window is split into the following subwindows: 126–135, 136–144, and 145–154 keV (Fig. 2B). In this way PER can be implemented on most current cameras for scatter removal in single monopeak isotope studies.

In the first versions of the PER application, a calibration procedure was necessary to integrate the nonuniformity of the EIRs over the field of view of the detector. This procedure consisted of acquiring a point source in air, at several meters from the uncollimated detector (*23*). However, in this study, a new calibration procedure, referred to as autocalibration (*24*), has been used. This procedure does not require any specific calibration acquisition and is based on the following principle. In each pixel, PER is successively performed using only 1 iteration for different EIR shifts ranging from −5 to +5 keV around the photopeak energy. The retained shift is that which minimizes the DIST between the DS and the RS. The complete iterative PER procedure is then performed on the pixel, integrating the retained EIR shift in Equations 2–4. It should be noted that the autocalibration procedure does not obviate checking the uniformity of the energy response of the detector. Regular checks will detect major (>5 keV) EIR shifts that preclude correct PER processing.

PER for Crosstalk Correction in Simultaneous ^{99m}Tc/^{201}Tl Imaging

Theory. Here, PER was applied only to the data recorded in the ^{201}Tl window centered on the isotope's main photopeak (62–89 keV). The higher photopeak window (167 keV) was not used, because it is essentially unaffected by ^{99m}Tc downscatter. A large (30%) ^{201}Tl window was chosen to collect most of the primary ^{201}Tl photons. Inside this window, the DS can be considered as a linear combination of the following 4 spectra: (a) the spectrum of the primary ^{201}Tl photons (PS); the spectrum of the scattered ^{201}Tl photons (SS); the spectrum of the downscattered ^{99m}Tc photons (and of the downscattered high-energy ^{201}Tl photons) (TS); and the spectrum of the collimator lead x-ray photons (CS). Then:

$$DS = p\,PS + s\,SS + t\,TS + c\,CS, \qquad \text{Eq. 6}$$

where p is the number of primary low-energy ^{201}Tl photons, s is the number of scattered low-energy ^{201}Tl photons, t is the number of downscattered ^{99m}Tc photons (plus downscattered high-energy ^{201}Tl photons), and c is the number of lead x-ray photons.

At the first iteration, PS and SS are determined as described above for single-isotope ^{99m}Tc imaging, using the multiple x-ray photons emitted by ^{201}Tl and their relative normalized intensity given by the decay table:

$$PS = 0.29\,EIR_{69} + 0.49\,EIR_{71} + 0.17\,EIR_{80} + 0.05\,EIR_{82}, \qquad \text{Eq. 7}$$

and

$$SS = 0.29\sum_{e=54}^{69} w1_e\,EIR_e + 0.49\sum_{e=54}^{71} w2_e\,EIR_e + 0.17\sum_{e=54}^{80} w3_e\,EIR_e + 0.05\sum_{e=54}^{82} w4_e\,EIR_e. \qquad \text{Eq. 8}$$

TS is determined in the same way:

$$TS = \sum_{e=54}^{96} w5_e\,EIR_e. \qquad \text{Eq. 9}$$

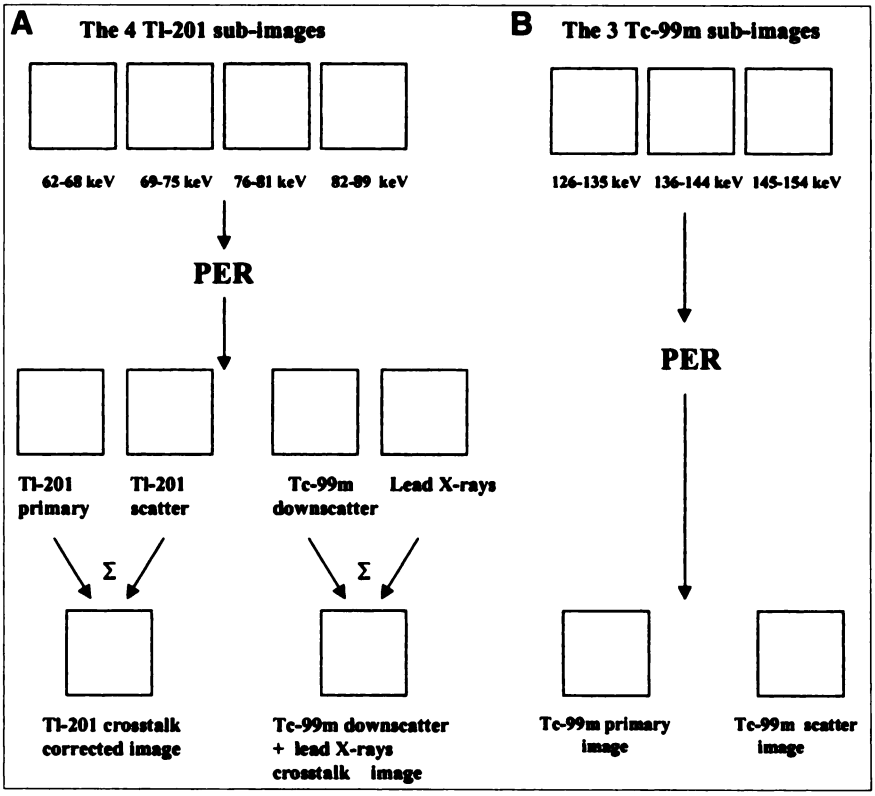

FIGURE 2. PER flow charts. (A) Four ^{201}Tl subwindow images are used for estimating ^{201}Tl crosstalk-corrected image and crosstalk image in simultaneous ^{99m}Tc/^{201}Tl imaging. (B) Three ^{99m}Tc subwindow images are used for estimating ^{99m}Tc primary image and ^{99m}Tc scatter image, in single ^{99m}Tc study and in simultaneous ^{99m}Tc/^{201}Tl study.

The values 54 and 96 keV are the lower- and higher-energy values, respectively, of the photons which contribute significantly to the 62–89 keV ^{201}Tl window.

CS is determined using the 4 main lead characteristic x-rays: 72, 75, 84, and 88 keV:

$$CS = w6_{72}\,EIR_{72} + w6_{75}\,EIR_{75} + w6_{84}\,EIR_{84} + w6_{88}\,EIR_{88}. \quad \text{Eq. 10}$$

Initial estimations of the coefficients p, s, t, and c are calculated applying linear regression to Equation 6 with the assumption that all the coefficients w_e, including the lead coefficients, are equal to 1 (uniform distribution). The iterative process is then undertaken as described above, to refine the shape of SS, TS, and CS. At step m, the RS will be:

$$^{m}RS = {}^{m}p\,PS + {}^{m}s\,{}^{m}SS + {}^{m}t\,{}^{m}TS + {}^{m}c\,{}^{m}CS, \quad \text{Eq. 11}$$

where ^{m}SS, ^{m}TS, and ^{m}CS are the estimates of SS, TS, and CS, respectively, at iteration m.

Figure 1B shows an example of ^{201}Tl DS and RS in 2 pixels extracted from the first projection of a ^{99m}Tc/^{201}Tl cardiac phantom SPECT study with 4 energy subwindows. One pixel is a high-count-level pixel located over the myocardium, and 1 is a low-count-level pixel located over the tissue background. As for the ^{99m}Tc spectra, this figure shows that the PER-modeled spectrum (RS) fits the DS well, both at low and high statistical noise levels.

Implementation. Four energy intervals (n = 4) have been chosen to provide for the 4 unknowns in Equation 6. In fact, splitting the 62- to 89-keV ^{201}Tl window into more subwindows could lead to a high statistical noise level in the subimages. The 62- to 89-keV window has then been split into the following subwindows: 62–68, 69–75, 76–81, and 82–89 keV (Fig. 2A). The autocalibration procedure has been applied using the same protocol as for ^{99m}Tc.

In practice, when simultaneous ^{99m}Tc/^{201}Tl imaging is performed, PER can be applied twice: once on the 3 ^{99m}Tc subwindows to separate the ^{99m}Tc photopeak image from the ^{99m}Tc scatter image, and once on the 4 ^{201}Tl subwindows to calculate the ^{201}Tl photopeak, ^{201}Tl scatter, ^{99m}Tc downscatter, and lead x-ray images. The sum of the ^{201}Tl photopeak and the ^{201}Tl scatter images is the ^{201}Tl crosstalk-corrected image. The sum of the ^{99m}Tc downscatter and the lead x-rays images is the crosstalk image (Fig. 2).

Validation

Planar Line Phantom. This phantom consists of 2 perpendicular sets of 10 parallel lines each. Lines were plexiglas tubes (length, 175 mm; diameter, 0.5 mm). All lines were fixed on a 10-mm–thick plexiglas sheet (300 × 300 mm). The in-plane distances between the lines of each set were as follows: 5, 7.5, 10, 12.5, 15, 20, 25, 30, and 50 mm. The plane of the lines was separated from the γ camera by a 100-mm–thick plexiglas sheet (300 × 300 mm). The vertical lines were filled with a 370 MBq ^{99m}Tc solution and the horizontal lines with a 74 MBq ^{201}Tl solution, giving a ^{99m}Tc/^{201}Tl ratio of 5 at time 0.

Seven successive planar acquisitions were recorded from time 0 to 48 h, moving neither the γ camera nor the phantom, corresponding to the following ^{99m}Tc/^{201}Tl ratios: 5, 4.5, 4.0, 3.5, 3.0, 2.5, and 0.031. All acquisitions were obtained with a DSX γ camera (SMVi, Buc, France) equipped with a parallel high-resolution collimator (high resolution, low energy). Each acquisition time was 900 s, except at 48 h when it was 1400 s to compensate for ^{201}Tl decay. The images were recorded in 128 × 128 matrices, without zoom. Seven spectral windows were used: the 4 ^{201}Tl subwindows described here and the 3 ^{99m}Tc subwindows (126–135, 136–144, and 145–154 keV) previously described (*23*). Because only 4 energy channels were available on the DSX γ camera, each acquisition was obtained in 2 steps: 1 with the 4 ^{201}Tl subwindows and the other with the 3 ^{99m}Tc subwindows. Because this study focused on the correction of ^{99m}Tc crosstalk into the ^{201}Tl images, PER was applied only to the 4 ^{201}Tl subwindows.

At each acquisition time, the results of PER processing comprised the following images: (a) unscattered + scattered primary ^{201}Tl photons (corrected image: p + s); and (b) scattered ^{99m}Tc photons + scattered high-energy ^{201}Tl photons + lead x-ray photons (crosstalk image: t + c).

The ^{201}Tl raw image was the summed image of the 4 ^{201}Tl subwindows. The ^{99m}Tc raw image was the summed image of the 3 ^{99m}Tc subwindows. The ^{201}Tl raw image at 48 h (^{99m}Tc/^{201}Tl = 0.031) was expected to contain ^{201}Tl events only (^{99m}Tc activity had essentially decayed by then) and was consequently referred to as the virgin ^{201}Tl image.

Contrast was measured using the count ratio [(Cmax − Cmin)/(Cmax + Cmin)], where Cmax and Cmin were the maximum and the minimum number of counts in a wide rectangular region of interest (ROI) centered on the upper horizontal line (this line is separated by 50 mm from the nearest adjacent horizontal line). Both line and background pixels were included in this ROI.

Noise was measured using the normalized SD (NSD), which was defined as the ratio of the SD and the mean calculated from a narrow ROI including only the upper horizontal line. Background pixels were not included in this ROI, because they were believed to contain only scattered events.

Cardiac SPECT Phantom. A thoracic phantom (Model ECT/Lung/P; Data Spectrum Corp., Hillsborough, NC) was used. It consists of a heart insert (Model ECT/CAR/I), 2 lung inserts, and a solid Teflon column simulating the spine. No liver insert was used, but a bowel "hot spot" was simulated using a 5-mL insert located under the heart. The total volume of the phantom was 9600 mL (with all the organs in place). Two solid transmural defects were included in the myocardial wall of the heart insert, 1 (2 mL) in the anterior wall and the other (1.5 mL) in the inferior wall. The phantom was filled at time 0 using the following activities: 185 MBq ^{99m}Tc and 37 MBq ^{201}Tl into the myocardial wall (^{99m}Tc/^{201}Tl ratio = 5); 370 MBq ^{99m}Tc and 74 MBq ^{201}Tl into the body of the phantom (^{99m}Tc/^{201}Tl ratio = 5); and 37 MBq ^{99m}Tc into the bowel hot spot. Water was added into the ventricle chamber and into the lungs, which also contained styrofoam beads.

Five successive SPECT acquisitions were recorded from time 0 to 46 h, without moving the γ camera or the phantom, corresponding to the following ^{99m}Tc/^{201}Tl ratios: 5.0, 3.9 (referred to as 4.0), 3.0, 2.2 (referred to as 2.0), and 0.04. The acquisitions were performed with a dual-head VERTEX γ camera (ADAC, Milpitas, CA) equipped with parallel high-resolution collimators (VXHR). SPECT studies were acquired over a 360° elliptical orbit using 64 projections and 128 × 128 matrices. No zoom was used. The acquisition time was 20 s/projection, except at 46 h, when it was 31 s to compensate for ^{201}Tl decay. The spectral windows were the same as those used for the planar line phantom. However, each acquisition had to be recorded in 3 steps, because only 3 energy channels were available on the VERTEX γ camera. Projections were corrected using PER in the same manner as for the planar line phantom.

Raw and corrected SPECT datasets were reconstructed after prefiltering with a 2-dimensional Butterworth filter of order 2.5,

cutoff 0.33 (^{99m}Tc) or order 5, cutoff 0.25 (^{201}Tl), using the same reconstruction limits, and were automatically reoriented using the same azimuth and elevation angles. All the short-axis datasets so derived were automatically and 3-dimensionally quantitated using the Cedars-Sinai quantitative perfusion SPECT (QPS) software (*25,26*), imposing the additional constraint of constancy for the apex-to-base distance between homologous ^{201}Tl and ^{99m}Tc images. All datasets were automatically divided in 20 segments, for each of which the following quantitative and semiquantitative parameters were calculated: (a) the quantitative average normalized pixel count in the segment (normalization was to the highest uptake pixel in the entire image); (b) the semiquantitative perfusion score, automatically calculated by the algorithm based on normal limits derived from a group of male patients undergoing separate rest ^{201}Tl–stress ^{99m}Tc sestamibi dual-isotope imaging (*26*). A 5-point (0–4 = normal-to-absent perfusion) scoring model was used. (c) The quantitative defect severity, or the number of SDs by which relative counts in each pixel were below the corresponding limit of normal in the database, averaged over all pixels in the segment; and (d) the quantitative defect extent, or the number of myocardial pixels having below-normal counts, expressed as a percentage of the myocardium.

Anterior and inferior defect contrast were defined as the ratio of the average quantitative pixel values in the normal segments and in the 2 anterior defect and 2 inferior defect segments, respectively.

The summed score, the average defect severity, and the average defect extent were computed over the entire myocardium for the ^{201}Tl images.

RESULTS

Planar Line Phantom

Figure 3 shows Tl-raw, Tl-PER, and Tc-raw planar images at the highest (5:1) and lowest (2.5:1) ^{99m}Tc/^{201}Tl ratios. The virgin ^{201}Tl image (Tl-raw image at 48 h, with ^{99m}Tc/^{201}Tl ≈ 0) is also presented. It can be seen that the ^{99m}Tc crosstalk or downscatter into the Tl-raw images is effectively corrected on the Tl-PER images. However, noise level appears to be slightly higher on the Tl-PER images than on the virgin ^{201}Tl image.

Figure 4A confirms the high ^{99m}Tc crosstalk contribution to the Tl-raw images, with a (^{99m}Tc + ^{201}Tl)/^{201}Tl ratio ranging from 336% for the 5:1 ^{99m}Tc/^{201}Tl ratio to 201% for the 2.5:1 ratio. PER processing substantially reduces this proportion to values from 128% to 108%, where 100% is the ideal value corresponding to no crosstalk. PER contrast enhancement is shown in Figure 4B, in which contrast is expressed as a percentage of the ideal contrast in the virgin ^{201}Tl image. Contrast in the PER-processed images is always >60% of that in the virgin ^{201}Tl image, compared with values of 15%–29% in the Tl-raw images, at the various ^{99m}Tc/^{201}Tl ratios. At high ^{99m}Tc/^{201}Tl ratios, the noise level in the Tl-PER images is substantially higher than on the virgin ^{201}Tl image (Fig. 4C), but the level abates at medium and low ratios. Moreover, it must be noted that NSD values on Tl-raw images are much higher, as a result of the heterogeneity generated by crosstalk of the scattered ^{99m}Tc photons coming from the vertical lines.

Cardiac SPECT Phantom

Figure 5 shows a 1-pixel–thick short-axis slice (Fig. 5A) and a 1-pixel–thick vertical long-axis slice (Fig. 5B) containing both the anterior and inferior defects. The blurring effect of crosstalk is clearly shown on the Tl-raw images for the different ^{99m}Tc/^{201}Tl ratios. The inferior defect is barely visualized on the Tl-raw image at the 5:1 ratio. PER greatly improves the visual assessment of the defects as well as the definition of the myocardial wall and the ventricular cavity, although the inferior defect remains slightly smoothed on the Tl-PER image at the highest ^{99m}Tc/^{201}Tl ratio. However, Tl-PER images are quite similar to the reference virgin ^{201}Tl

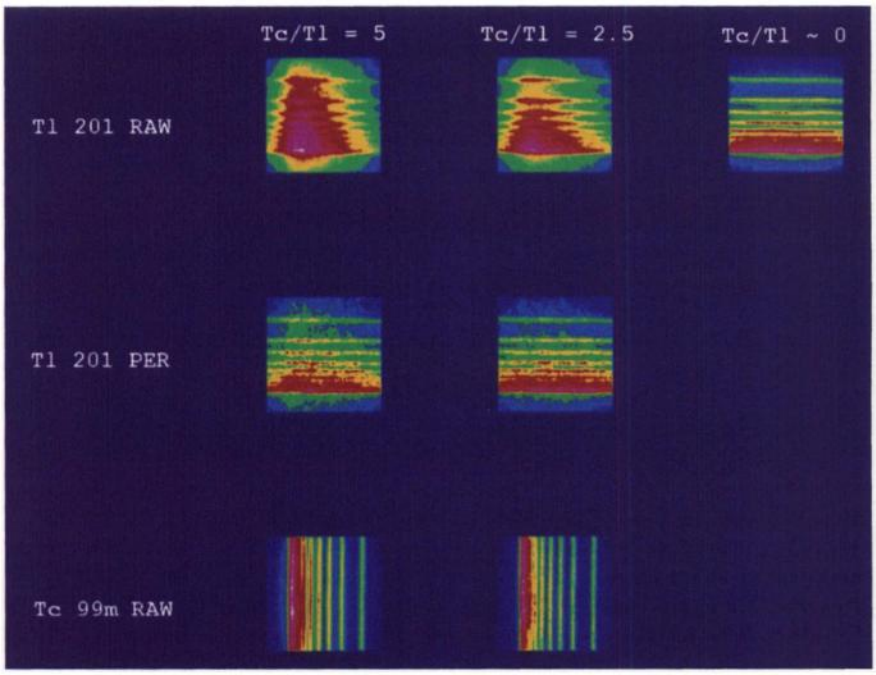

FIGURE 3. Planar line phantom. Tl-raw, Tl-PER, and Tc-raw images at highest (5:1) and lowest (2.5:1) ^{99m}Tc/^{201}Tl ratios. Tl-raw image at ^{99m}Tc/^{201}Tl ratio ≈ 0 is virgin Tl image.

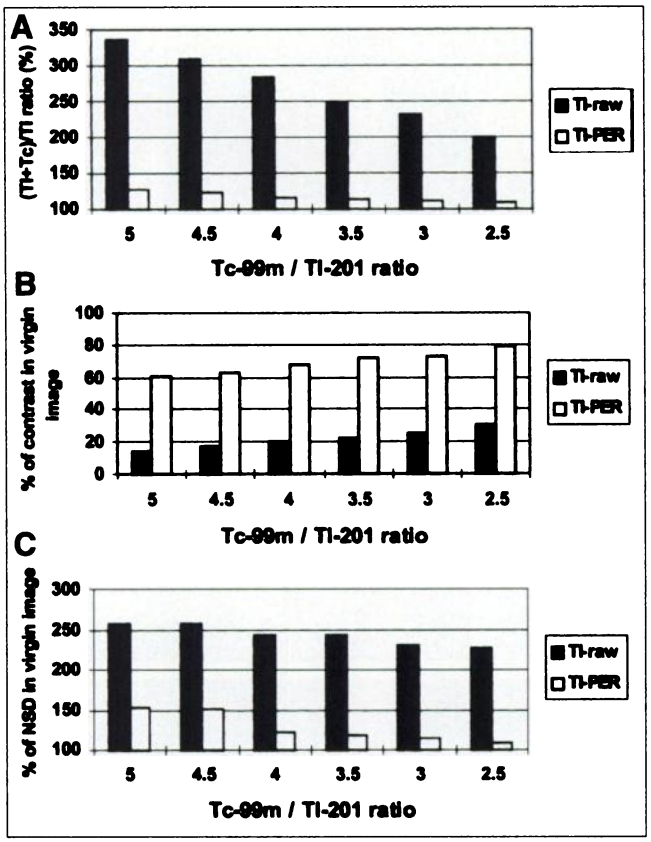

FIGURE 4. Planar line phantom. Total number of counts (A), contrast (B), and NSD (C) in raw and PER-corrected ^{201}Tl images compared to reference virgin ^{201}Tl image for different ^{99m}Tc/^{201}Tl ratios. Ideal value is 100 in all graphs.

image. Only minor differences exist between the Tc-raw images, as a result of the weak ^{201}Tl crosstalk into the ^{99m}Tc images.

Figure 6 shows the substantial defect contrast enhancement in Tl-PER images. Anterior and inferior defect contrasts range from 1.18 to 1.22 and from 1.12 to 1.16, respectively, for Tl-raw images versus 1.28 to 1.32 and 1.21 to 1.24, respectively, for Tl-PER images. The reference anterior and inferior defect contrasts calculated on the virgin ^{201}Tl image are 1.31 and 1.25 respectively. In the ^{99m}Tc images, the contrast is significantly higher, because anterior and inferior values range from 1.62 to 1.64 and 1.43 to 1.36, respectively. This is the result of the greater photon energy of the ^{99m}Tc photons. Contrast recovery in the Tl-PER images is slightly better at the lowest ^{99m}Tc/^{201}Tl ratios.

Table 1 shows the summed score, the average severity, and the average extent calculated over the entire myocardium for the ^{201}Tl images. Without PER processing, defects are severely underestimated by the Tl-raw images. PER-corrected images, by comparison, are much closer to the reference ^{201}Tl virgin images.

DISCUSSION

Several subtraction techniques have already been proposed for crosstalk correction in simultaneous dual-isotope imaging. One technique involves a two-step acquisition procedure (*15*): ^{99m}Tc is first imaged in its own window as well as in that of ^{201}Tl, then ^{201}Tl is administered and simultaneous dual imaging of ^{99m}Tc and ^{201}Tl is performed. Finally, the first ^{99m}Tc image in the ^{201}Tl window is subtracted from the dual or contaminated ^{201}Tl image. The major problem with this approach is the registration of these 2 images, which are acquired in the same window but at separate times. Other methods (*18–20*) aim at estimating the ^{99m}Tc crosstalk into the ^{201}Tl window using an additional image recorded in the energy range of the scattered ^{99m}Tc photons, i.e., 80–140 keV. Some methods use the conventional ^{99m}Tc 140-keV image itself for this estimation (*6,9,10*). In that case, a fraction (referred to as crosstalk fraction) of this crosstalk image will then be subtracted from the ^{201}Tl image to get the crosstalk-free image. A major difficulty of this approach is clearly the accurate determination of the crosstalk fraction, which is greatly depth- and object-dependent. Regression equations, based on preliminary Monte Carlo and phantom studies, have been proposed (*20*) for this calculation, but they are empirical and must be reformulated for each specific acquisition procedure. In addition, it is not realistic to assume that the distribution of the scattered ^{99m}Tc photons in the scatter window is the same as that in the ^{201}Tl window, because the scatter angles and the scatter orders are functions of the energy of the photon.

Another approach to crosstalk subtraction is to measure the ^{99m}Tc point–spread function (PSF) in the ^{201}Tl window using a water phantom and then perform a spatial deconvolution on the ^{201}Tl images (*2,21*). However, this procedure is an ill-conditioned problem that requires regularization techniques and low-pass filters (the numerical parameters of which are often chosen in an empirical way). Moreover, the PSF should theoretically be measured for different water depths and for different acquisition systems and protocols, which is difficult to do in practice.

Nakamura et al. (*27*) have reported on the clinical feasibility of the correction method of Moore et al. (*28*), a subtractive technique in which the crosstalk image is estimated by a linear combination of an image recorded between 90 and 110 keV and of the ^{99m}Tc photopeak image. These 2 images are first blurred by a smoothing filter. In practice, the technique requires only simultaneous acquisition in 4 energy windows, but preliminary phantom data must be acquired to determine the appropriate parameters of the filters and the weights in the linear combination. In theory, this calibration should be performed before each specific acquisition.

The main limitation of this technique probably is the assumption that a smoothing filter is able to transform the 90- to 110-keV downscatter image and the photopeak image into the 62- to 84-keV downscatter image. In fact, there is no physical reason to suppose that the variation of scatter angles and scatter orders with energy can be modeled by a smoothing filter.

In this study, we propose an alternative crosstalk correction technique based on the PER method, already developed

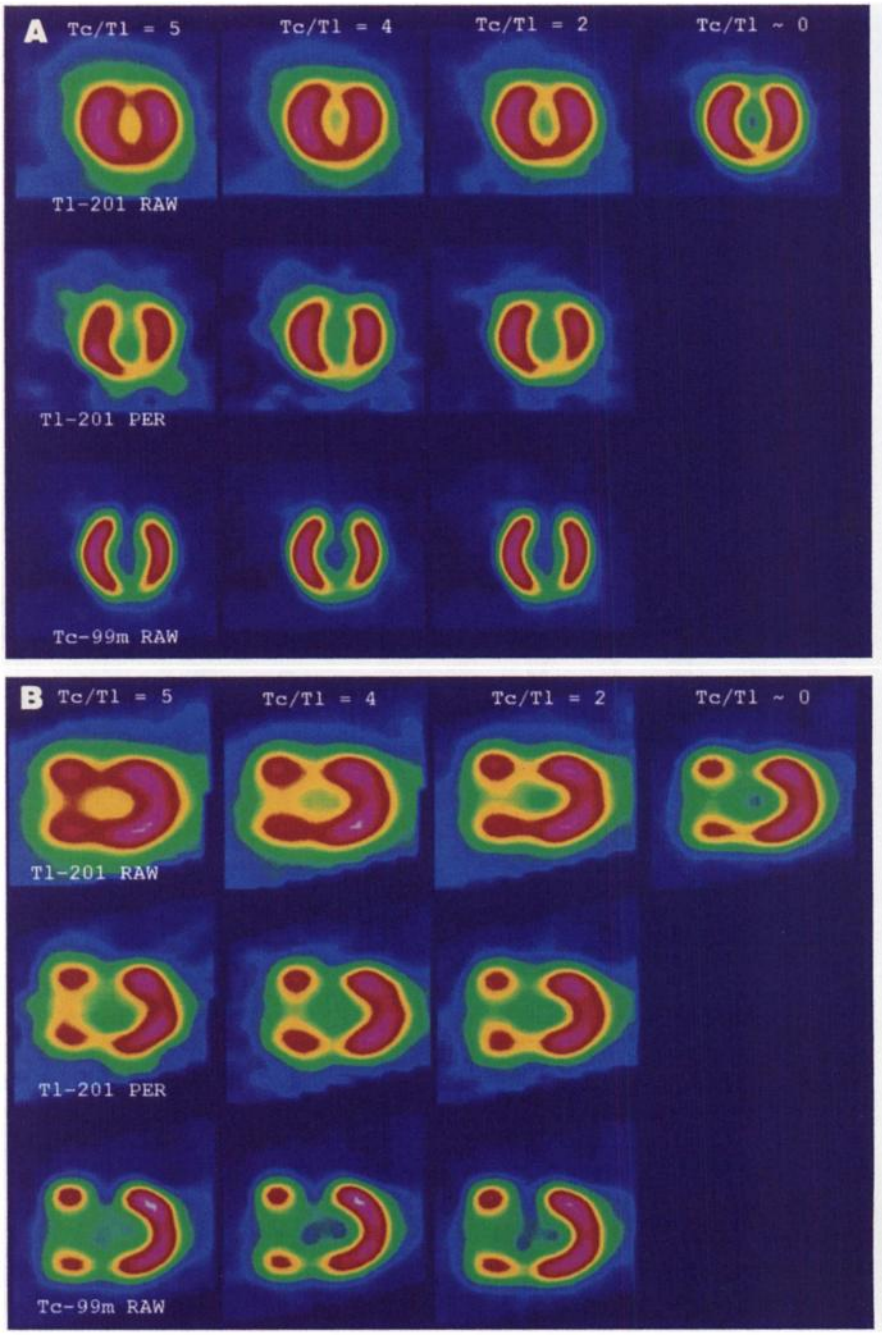

FIGURE 5. (A) Cardiac SPECT phantom. ^{201}Tl-raw, ^{201}Tl-PER, and ^{99m}Tc-raw short-axis slices at 3 ^{99m}Tc/^{201}Tl ratios. ^{201}Tl-raw slice at ^{99m}Tc/^{201}Tl ratio ≈ 0 is virgin ^{201}Tl slice. (B) Cardiac SPECT phantom. ^{201}Tl-raw, ^{201}Tl-PER, and ^{99m}Tc-raw vertical long-axis slices at 3 ^{99m}Tc/^{201}Tl ratios. ^{201}Tl-raw slice at ^{99m}Tc/^{201}Tl ratio ≈ 0 is virgin ^{201}Tl slice.

and validated with respect to scatter removal in single ^{99m}Tc acquisitions (*22,23*). The underlying assumption is that scatter and crosstalk can both be considered as contaminant spectra of a spectrum of interest. In single monopeak radionuclide studies, the spectrum of interest is that of the primary photons, and the contaminant spectrum is that of the scattered photons. In ^{99m}Tc/^{201}Tl studies, the spectrum of interest is that of the ^{201}Tl photons, and the contaminant spectra are those of scattered ^{99m}Tc, high-energy ^{201}Tl and lead-characteristic x-ray photons. PER's goal is to extract a spectrum of interest from a DS that is the sum of several spectra. The main advantage of PER is that it does not require any assumptions about the distribution of the scattered ^{99m}Tc photons in the ^{201}Tl image. Moreover, the technique uses a spectral deconvolution procedure with few equations (i.e., energy windows) and few unknown variables (i.e., energy spectra) and can thus be performed on a pixel-by-pixel basis.

The results of this study confirm the high level of contaminant photons into the ^{201}Tl windows, as already reported by several groups (*13,14,16*). PER correction of crosstalk is shown in Figures 3 and 5, resulting in images qualitatively close to the corresponding virgin ^{201}Tl images. On a quantitative basis, PER correction was found to increase greatly both the proportion of ^{201}Tl photons in the ^{201}Tl window and the overall image contrast in planar

images acquired with both isotopes on board, compared with no correction (Figs. 4A and B). There are small differences between the Tl-PER and the reference virgin ^{201}Tl values that decrease with the ^{99m}Tc/^{201}Tl ratio. The overall noise level in the Tl-PER images is also much less than that in the Tl-raw images, although Tl-PER images are noisier than the virgin ^{201}Tl image to a degree proportional to the ^{99m}Tc/^{201}Tl ratio.

With respect to the cardiac SPECT phantom results, PER's ability to correct for isotope crosstalk depends on the ^{99m}Tc/^{201}Tl ratio, as measured by anterior and inferior defect contrast in Figure 6. However, even for the highest ratio, the contrast recovery in Tl-PER image seems largely satisfactory, because it is well shown on the slices shown in Figure 5. Moreover, all the values of the QPS parameters (Table 1) derived from Tl-PER images are close to the virgin ^{201}Tl values. With a myocardial extraction of 73% for ^{201}Tl and 40% for ^{99m}Tc-sestamibi and a fraction of 4% of the cardiac output perfusing the myocardium at rest and 5% at stress (*17*), a ^{99m}Tc/^{201}Tl ratio of 5:1 corresponds to an administration of 945 MBq ^{99m}Tc-sestamibi at stress and 130 MBq ^{201}Tl at rest. This means that PER processing of simultaneous ^{99m}Tc/^{201}Tl studies does not preclude the use of the relatively high ^{99m}Tc-sestamibi activities often associated with gated SPECT acquisitions (*29*).

The QPS parameters listed in Table 1 were calculated using separate dual-isotope normal limits developed in a male patient population and will not perfectly extrapolate to a phantom. However, these limits must be considered here as reference values to simultaneously compare Tl-raw, Tl-PER, and ^{201}Tl virgin images.

PER correction of crosstalk in the ^{201}Tl images requires 4 energy subwindows. In addition, 3 ^{99m}Tc subwindows must be added to simultaneously apply PER for separating the primary ^{99m}Tc photons from the scattered ones, i.e., data must be acquired simultaneously in 7 energy windows. Because this is not yet possible on the γ camera used in this study (as well as in a majority of commercial systems), successive acquisitions were performed, which was feasible in a phantom experiment but would be impractical with patients. Clinical validations necessary for the PER technique will require the ability to acquire data in several energy windows.

TABLE 1
Summed Perfusion Score, Average Defect Severity, and Average Defect Extent Calculated over Entire Myocardium

	Summed score		Average defect severity*		Average defect extent†	
Tc/Tl ratio	Tl-raw	Tl-PER	Tl-raw	Tl-PER	Tl-raw	Tl-PER
5	4	8	0.40	0.59	4.7	7.4
4	5	8	0.48	0.61	5.5	7.6
3	5	8	0.44	0.75	5.2	7.9
2	5	9	0.52	0.79	5.9	8.8
0 (Tl virgin)	9		0.73		8.7	

*In number of SDs.
†In percentage of whole myocardium.

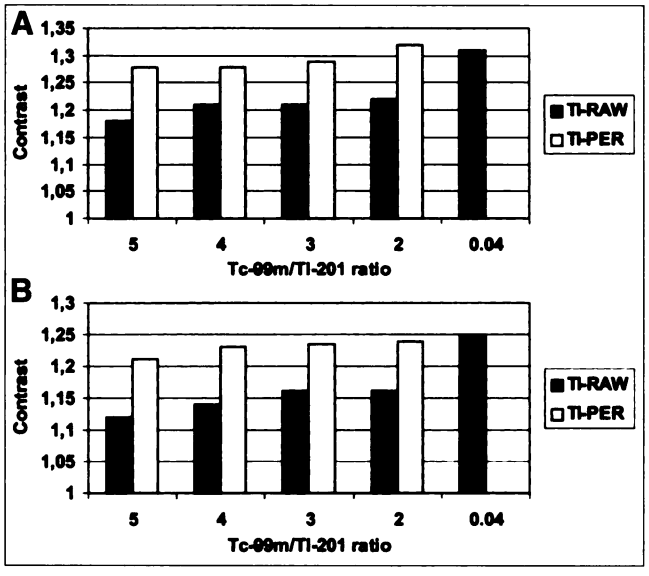

FIGURE 6. Cardiac SPECT phantom. Anterior (A) and inferior (B) defect contrast in raw and PER-corrected ^{201}Tl images. At ratio 0.04, raw ^{201}Tl image is essentially virgin ^{201}Tl image.

CONCLUSION

This study has shown that PER spectral deconvolution enables the removal of ^{99m}Tc downscatter photons from images acquired in ^{201}Tl windows when both ^{99m}Tc and ^{201}Tl are present. Its performance has been assessed quantitatively using a planar line phantom and a cardiac SPECT phantom at different ^{99m}Tc/^{201}Tl ratios. The results remain to be confirmed on patient series.

ACKNOWLEDGMENT

The authors are grateful to Joshua Anah for his help in the revision of the manuscript.

REFERENCES

1. Links JM. Simultaneous dual-radionuclide imaging: are the images trustworthy [editorial]? *Eur J Nucl Med.* 1996;23:1289–1291.
2. Knesaurek K, Machac J. Enhanced cross-talk correction technique for simultaneous dual-isotope imaging: a Tl-201/Tc-99m myocardial perfusion SPECT dog study. *Med Phys.* 1997;24:1914–1923.
3. Berman DS, Kiat H, Friedman JD, et al. Separate acquisition rest thallium-201/stress technetium-99m sestamibi dual-isotope myocardial perfusion SPECT: a clinical validation study. *J Am Coll Cardiol.* 1993;22:1455–1464.
4. Constantinesco A, Mertz L, Brunot B. Myocardial perfusion and function imaging at rest with simultaneous thallium-201 and technetium-99m blood-pool dual-isotope gated SPECT. *J Nucl Med.* 1997;38:432–437.
5. Asano H, Sone T, Tsuboi H, et al. Diagnosis of right ventricular infarction by overlap images of simultaneous emission computed tomography using technetium-99m pyrophosphate and thallium-201. *Am J Cardiol.* 1993;71:902–908.
6. Neumann DR. Simultaneous dual-isotope SPECT imaging for the detection and characterization of parathyroid pathology. *J Nucl Med.* 1992;33:131–134.
7. Mochizuki T, Takechi T, Murase K, et al. Thallium-201/technetium-99m-phytate (colloid) subtraction imaging of hepatocellular carcinoma. *J Nucl Med.* 1994;35:1134–1137.

8. de la Peña NC, Ketonen L, Villanueva-Meyer J. Imaging of brain tumors in AIDS patients by means of dual-isotope thallium-201 and technetium-99m sestamibi single-photon emission tomography. *Eur J Nucl Med.* 1998;25:1404–1411.
9. Frey EC, Tsui BMW, Perry JR. Simultaneous acquisition of emission and transmission data for improved thallium-201 cardiac SPECT imaging using a technetium-99m transmission source. *J Nucl Med.* 1992;33:2238–2245.
10. Ficaro EP, Fessler JA, Rogers WL, Schwaiger M. Comparison of americium-241 and technetium-99m as transmission sources for attenuation correction of thallium-201 SPECT imaging of the heart. *J Nucl Med.* 1994;35:652–663.
11. DePuey EG. Simultaneous thallium-201/technetium-99m dual isotope cardiac SPECT: ready for prime time [editorial]? *J Nucl Med.* 1993;11:2006–2008.
12. Lowe VJ, Greer KL, Hanson MW, Jaszczak RJ, Coleman RE. Cardiac phantom evaluation of simultaneously acquired dual isotope rest thallium-201/stress technetium-99m SPECT images. *J Nucl Med.* 1993;34:1998–2006.
13. Unlu M, Gunaydin S, Ilgin N, Inanir S, Gokcora N, Gokgoz L. Dual isotope myocardial perfusion SPECT in the detection of coronary artery disease: comparison of separate and simultaneous acquisition protocols. *J Nucl Biol Med.* 1993;37:233–237.
14. Kiat H, Germano G, Friedman J, et al. Comparative feasibility of separate or simultaneous rest thallium-201/stress technetium-99m-sestamibi dual-isotope myocardial perfusion SPECT. *J Nucl Med.* 1994;35:542–548.
15. Weinstein H, King MA, Reinhardt CP, McSherry BA, Leppo JA. A method of simultaneous dual-radionuclide cardiac imaging with technetium-99m and thallium-201. I: analysis of interradionuclide crossover and validation in phantoms. *J Nucl Cardiol.* 1994;1:39–51.
16. Cao ZJ, Chen CC, Maunoury C, Holder LE, Abraham TC, Tehan A. Phantom evaluation of simultaneous thallium-201/technetium-99m acquisition in single-photon emission tomography. *Eur J Nucl Med.* 1996;23:1514–1520.
17. Kwok CG, Wu S, Tsang P, Strauss W. Feasibility of simultaneous dual-isotopemyocardial perfusion acquisition using a lower dose of sestamibi. *Eur J Nucl Med.* 1997;24:281–285.
18. Moore SC, Syravanh C, Tow DE. Simultaneous SPECT imaging of Tl-201 and Tc-99m using four energy windows [abstract]. *J Nucl Med.* 1993;34(suppl):188P.
19. Yang DC, Ragaza E, Gould L, et al. Radionuclide simultaneous dual-isotope stress myocardial perfusion study using the "three window technique." *Clin Nucl Med.* 1993;18:852–857.
20. Hademenos GJ, Dahlbom M, Hoffman EJ. Simultaneous dual-isotope technetium-99m/thallium-201 cardiac SPET imaging using a projection-dependent spilldown correction factor. *Eur J Nucl Med.* 1995;22:465–472.
21. Knesaurek K. A new dual-isotope convolution cross-talk correction method: a Tl-201/Tc-99m SPECT cardiac phantom study. *Med Phys.* 1994;21:1577–1583.
22. Hannequin P, Mas J. Photon energy recovery: a method to improve the effective energy resolution of gamma cameras. *J Nucl Med.* 1998;39:555–562.
23. Hannequin P, Mas J. Calibration procedure and quantitative validation of photon energy recovery for scatter removal in daily practice [abstract]. *J Nucl Med.* 1998;39(suppl):175P.
24. Hannequin P, Vinot S, Mas J. Photon energy recovery (PER) auto-calibration for Tc-99m and Tl-201 scatter removal [abstract]. *J Nucl Med.* 1999;40(suppl):304P.
25. Germano G, Kavanagh PB, Waechter P, et al. A new automatic approach to myocardial perfusion SPECT quantitation [abstract]. *J Nucl Med.* 1998;39(suppl): 62P.
26. Sharir T, Germano G, Kavanagh PB, et al. A novel method for quantitative analysis of myocardial perfusion SPECT: validation and diagnostic yield [abstract]. *J Nucl Med.* 1998;39(suppl):103P.
27. Nakamura M, Takeda K, Ichihara T, et al. Feasibility of simultaneous stress ^{99m}Tc-sestamibi/rest ^{201}Tl dual-isotope myocardial perfusion SPECT in the detection of coronary artery disease. *J Nucl Med.* 1999;40:895–903.
28. Moore SC, English RJ, Syravanh C, et al. Simultaneous Tc-99m/Tl-201 imaging using energy-based estimation of the spatial distributions of contaminant photons. *IEEE Trans Nucl Sci.* 1995;44:1189–1195.
29. Germano G, Kiat H, Kavanagh PB, et al. Automatic quantification of ejection fraction from gated myocardial perfusion SPECT. *J Nucl Med.* 1995;36:2138–2147.